ORIGINAL ARTICLE

Trabecular meshwork failure in a model of pigmentary glaucoma

Short running head: An ex vivo pigmentary glaucoma model

Yalong Dang[1], Susannah Waxman[1], Chao Wang[1, 2, 3], Ralista Loewen[1], Ming Sun[4] and Nils Loewen[1]

1: Department of Ophthalmology, School of Medicine, University of Pittsburgh, Pittsburgh, United States of America

2: Department of Ophthalmology, Xiangya Hospital, Central South University, Changsha, China

3: The Third Xiangya Hospital of Central South University, Changsha, Hunan, China.

4: Department of Cell Biology, School of Medicine, University of Pittsburgh, Pittsburgh, United States of America

*** Corresponding author:**
Nils A. Loewen, MD, PhD
203 Lothrop St
Suite 819
Pittsburgh, PA 15213
Email: Loewen.nils@gmail.com
Phone: 412-605-1541

Abstract

Pigment dispersion syndrome can lead to pigmentary glaucoma (PG), a poorly understood condition of younger, myopic eyes with fluctuating, high intraocular pressure (IOP). The absence of a model similar in size and behavior to human eyes has made it difficult to investigate the pathophysiology of IOP, pigment and phagocytosis. Here, we present a porcine ex vivo model that recreates the features of PG consisting of intraocular hypertension, pigment accumulation in the trabecular meshwork and failure of phagocytosis. In in vitro and ex vivo eye perfusion cultures we found that the trabecular meshwork (TM) cells that regulate outflow form of actin stress fibers, have a decreased phagocytosis and increased migration. Gene microarray and pathway analysis suggested key roles of RhoA and tight junctions in regulating the TM cytoskeleton, motility, and phagocytosis thereby providing new targets for future PG therapy.

Keywords: pigmentary glaucoma; Intraocular pressure; Trabecular meshwork; Cytoskeleton; Phagocytosis, Gene microarray, Signal pathway.

Introduction

Pigmentary glaucoma (PG) is a form of secondary open angle glaucoma in myopic eyes that affects patients in their 30s; individuals often experience a high, fluctuating intraocular pressure (IOP) with an increased resistance to nonsurgical treatment compared to primary open angle glaucoma[1,2]. In addition to a baseline dispersion of pigment, pigment showers can be triggered by physical activity or eye movements in some subjects but often remain asymptomatic, making this condition particularly vexing. First described by Sugar and Barbour in 1949[3], the clinical hallmark of pigment release is readily apparent with transillumination of the mid-peripheral iris (Fig. 1), deposition of pigment on the corneal endothelium (Krukenberg spindle) and in the trabecular meshwork (TM)[4] yet the pathogenesis remains poorly understood. Although the amount of pigment granules in the aqueous humor is correlated to IOP[5], a simple physical obstruction to outflow does not appear to be the cause of increased IOP. DBA/2J[6] and Col18a1(-/-) mice[7] have been used as models of PG but their shortcomings are a mixed mechanism form of both angle closure and pigment dispersion[6] and lack of ocular hypertension[7], respectively. Rodent models also lack the size and multilayered architecture that TM has in larger mammals[8].

Our prior work took advantage of the availability of pig eyes and an anatomy of the angular aqueous plexus[9] that matches several features of the human outflow tract[10–13]; we established gene transfer[12,14], modeled segmental outflow[11,15,16] and created a microincisional angle surgery system[17–19].

We hypothesized that pigment dispersion in perfused pig eyes would cause TM failure with an increased IOP. The aim of this study was to develop a standardized and accessible PG model that allows to study TM function and signal pathway changes to identify new treatment targets.

Results

We developed a porcine eye model of PG by replicating the clinical features in human patients: individuals with PG have a higher concentration of pigment granules in the aqueous humor[5], inside of TM cells[20–22], and experience a migration of these cells[20,21].

Pigment granules lack cytotoxicity to primary TM cells. We produced pigment granules of 1.03±0.11 micron that were similar to pigment in human pigmentary glaucoma by subjecting porcine iris pigment epithelium to freeze-thaw cycles. Stocks could be kept at a concentration of $4.3x10^9$ particles/ml for up to 1 month **(Fig. 1A)**. Primary TM cells obtained from freshly prepared TM exhibited the characteristic spindle-shaped morphology and were phagocytotically active. They expressed TM specific markers, MGP, AQP1 and alpha-SMA **(Fig. 1B)**.

The cytotoxicity of pigment granules was evaluated by flow cytometry and immunostaining using calcein AM and PI co-labelling. Viable TM cells can convert non-fluorescent calcein AM to green fluorescent calcein by intracellular esterase, but do not allow propidium iodide (PI) entrance or binding of nucleic acids[23]. Pigment granules at 1.67 x 10^7 particles/ml neither increased the percentage of PI labelled apoptotic or dead cells ((0.00±0.00)% in the pigment group vs (0.27±0.07)% in the normal control, P>0.05) nor decreased the percentage of calcein labelled viable cells ((84.90±3.87)% in the pigment group compared to (84.57±3.00)% in the normal control, P>0.05) **(Fig. 1C)**.

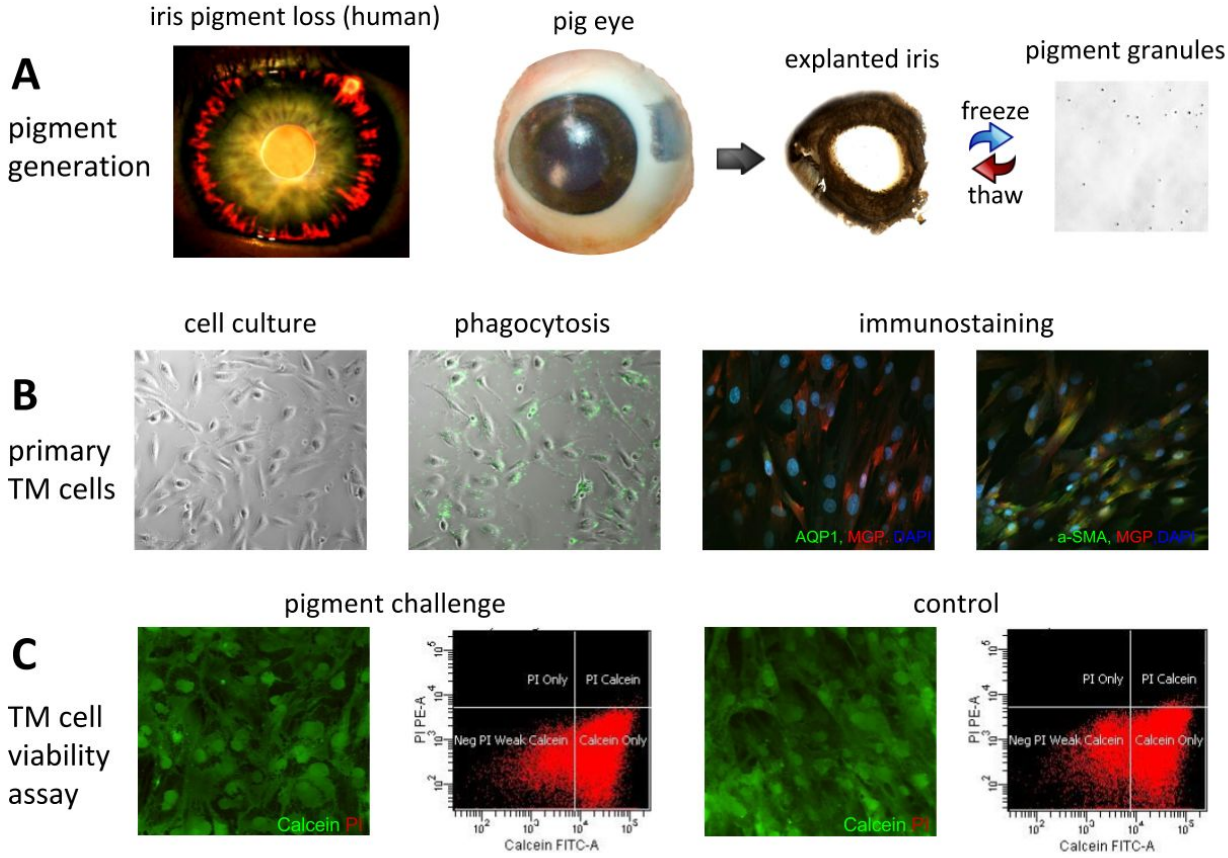

Figure 1: Pigment generation and in vitro exposure to pigment dispersion. In the human eye with pigment dispersion, pigment and eventually stroma is lost in the midperiphery of the iris (transillumination, A, left). Similar pigment granules of can be generated by exposing an explanted pig iris to freeze-thaw cycles (A, middle and right). Granules had an even size of 1.03 ± 0.11 micron (A, right, hemocytometer). Isolated primary trabecular meshwork (TM) cells from pig eyes (B, left to right) displayed the characteristic morphology, phagocytotic activity (fluorescent microspheres) and immunostaining pattern of TM specific markers, MGP, AQP1 and alpha-SMA (B, right). Exposure to to pigment did not change the percentage of viable cells ((84.90 ±

3.87)% in the pigment group compared to (84.57 ± 3.00)% in the normal control, P>0.05) or PI-positive, dead or apoptotic cells (C).

Pigment elevates intraocular pressure. Eight left-right matched porcine anterior segment pairs were randomly assigned to the pigment or the control group, respectively. Similar baseline IOPs were established for 72 hours (11.80±0.78 mmHg vs 11.64±0.51 mmHg, *P*= 0.872), followed by 180 hours of pigment exposure at a concentration of $1.67x10^7$ particles/ml, or a sham treatment with normal tissue-culturing medium. The control group did not have any significant change of IOP throughout the experiment (all *P*>0.05). In contrast, pigment resulted in an IOP elevation that became significantly higher at 24 hours, peaked at 96 hours at 23.0±6.0 mmHg and persisted at an IOP 75% above the baseline of 11.5±0.8 mmHg (all *P*<0.05, compared to group average baseline). Pigment dispersion eyes had a significantly greater IOP fluctuation than controls (1.78±0.16 vs 0.83±0.05, *P*<0.001), indicating different IOP responses of individual eyes to pigment treatment existed **(Fig. 2)**.

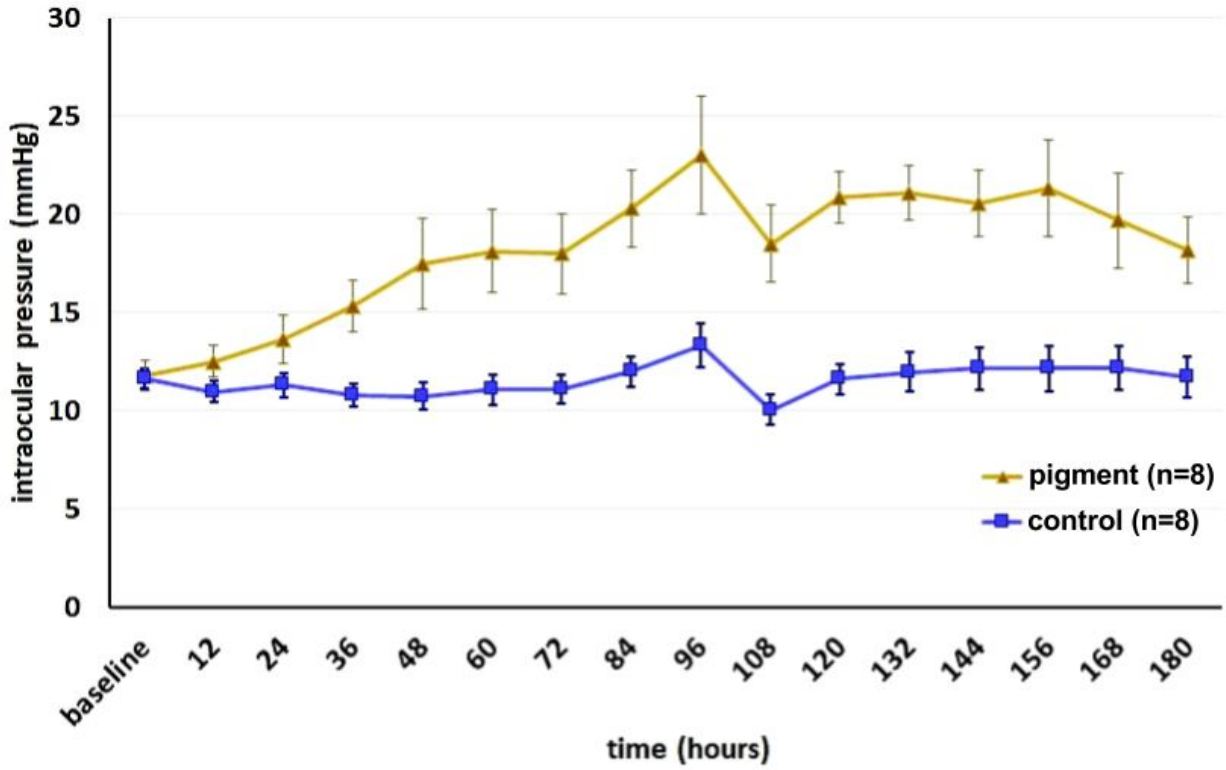

Figure 2. IOP elevation following pigment dispersion. IOP of perfused anterior segments starting to increase after 48 hours (P=0.026) and persisted for the remainder of the study (all P<0.05). IOP fluctuation in the pigment group was significantly larger than in the paired controls (P<0.001). A media change occurred after the 96 hour time point.

Lysosome and phagosome activated by pigment. Anterior segments of control eyes presented with a normal TM consisting of the uveal , corneoscleral, and cribriform meshwork immediately adjacent to the inner wall of Schlemm's canal like segments of the angular aqueous plexus **(Fig. 3A)**. Only occasional, scattered pigment was seen that was intracellular **(Fig. 3I, red arrowhead)**. In contrast, pigment dispersion eyes contained numerous TM cells with intracytoplasmic pigment granules, including enlarged cells that were protruding into elements of the downstream outflow tract **(Fig. 3B, C, F, G, J, K, read arrowheads)**. There was no evidence of collapse of intertrabecular spaces or a physical pigment obstruction the TM or collector channels **(Fig. 3B and C)**. Ultrastructurally, pigment induced the activation of lysosomes and phagosomes both in vitro and ex vivo **(Fig. 3K and L, blue arrowheads)**. Numerous pigment granules appeared ingested and at different stages of hydrolysis by secondary lysosomes **(Fig. 3K L)**. A swollen and distended endoplasmic reticulum could also frequently be seen in these eyes **(Fig. 3J, K and L, yellow arrowheads)**.

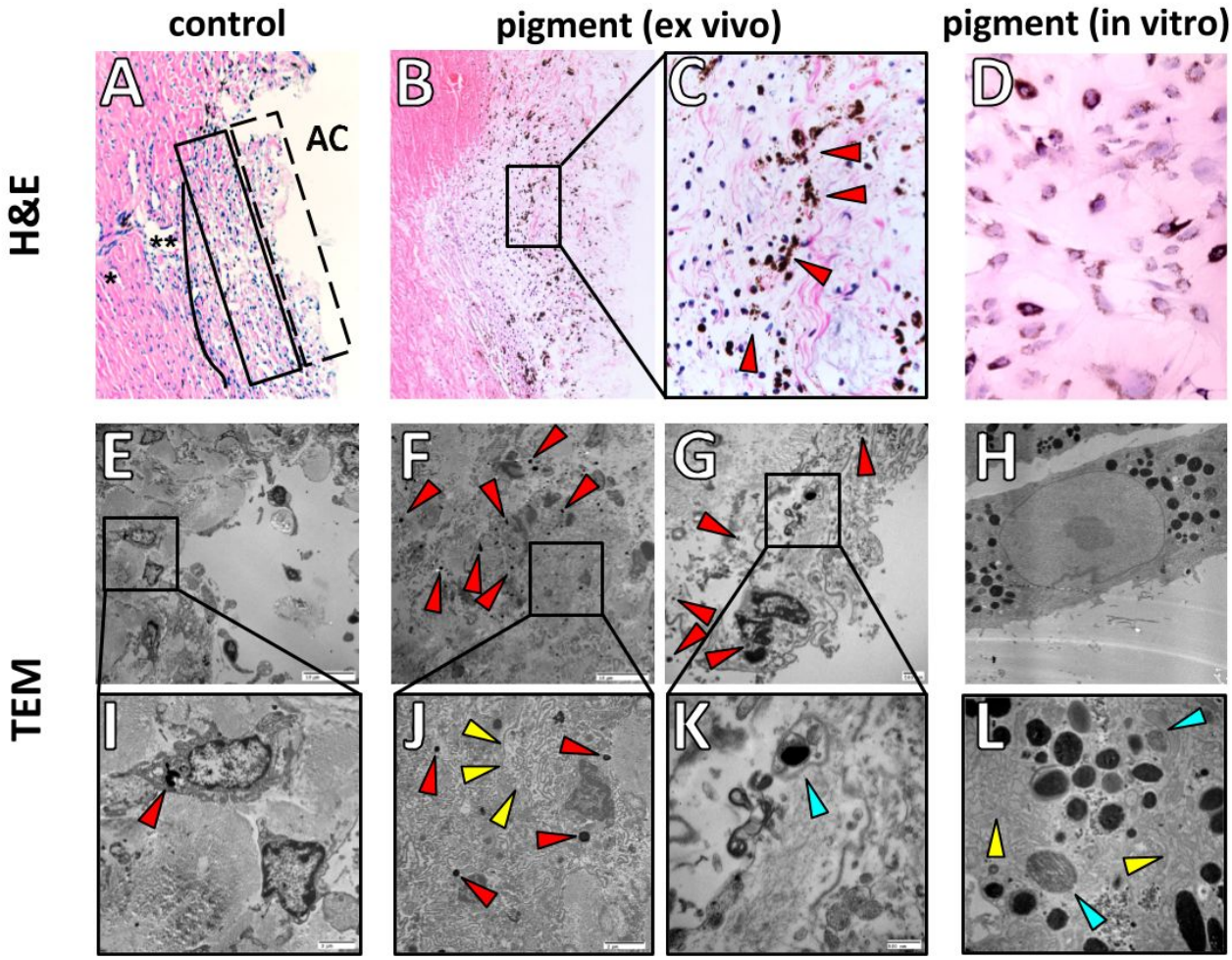

Figure 3. Ultrastructure and histology of the trabecular meshwork (TM). The TM consisted of three characteristic layers: the uveal meshwork (dashed line box, Figure 3A), the corneoscleral meshwork (solid line box, Figure 3A) and the juxtacanalicular meshwork (solid line, Figure 3A), adjacent to the inner wall of Schlemm's canal (SC) (Figure 3A, black stars). The outer layers were phagocytotically active. Pigment granules were located within cells and around the nucleus in the ex vivo model (Figure 3B and 3C, red arrows) and in vitro (Figure 3D, red arrows). Transmission electron microscopy showed occasional pigment in normal TM (Figure 3E and 3I, red arrows), and a larger number in the inner TM layers (Figure 3F and Figure 3J, red arrows), the outer TM layers (Figure 3G and 3K, red arrows) and in primary TM cells (Figure 3H). Pigment hydrolysis in different phagolysosome stages (Figure 3K and 3L, Blue arrows) and endoplasmic reticulum (Figure 3J and 3L, Yellow arrows) were also seen in vitro and ex vivo.

Declining phagocytosis, motility and cytoskeleton disruption. The reorganization of the cytoskeleton[24], decrease of phagocytosis[25,26] and increase of motility[20,21], features are closely related to regulation of outflow[27], were three most notable observations in eyes exposed to pigment. Different from the in vitro cell body contraction of the dexamethasone treated positive control group **(Fig. 4 B4, 100 nM)**, pigment did not cause a significant morphological change at day 1 and 7 in primary TM cells **(Fig. 4 B2-3)**.

We used F-actin to label the cytoskeleton of TM cells. The earliest changes of the F-actin cytoskeleton by the pigment treatment included polymerization of F-actin microfilaments and formation of stress fiber bundles **(white arrowheads, Fig. 4B2 and 3)**. These stress fibers further polymerized and became long, thick, filamentous bundles at day 7 **(Fig. 4B3)**. Similarly, 100 nM dexamethasone also induced thick F-actin stress bundles **(Fig. 4B4, write arrowheads)** at day 7, but with many nest-like actin networks, not the cross-linked actin networks (CLANs) as reported in human TM cells[28]. Consistent with in vitro

findings, F-actin microfilaments in normal TM flat-mounted tissue samples showed weak, spot-like or segmental stainings **(Fig. 4C1 and 2)**, contrasting the thick, bundle-like, continuous stress fibers in the pigment group **(Fig. 4C3 and 4)**.

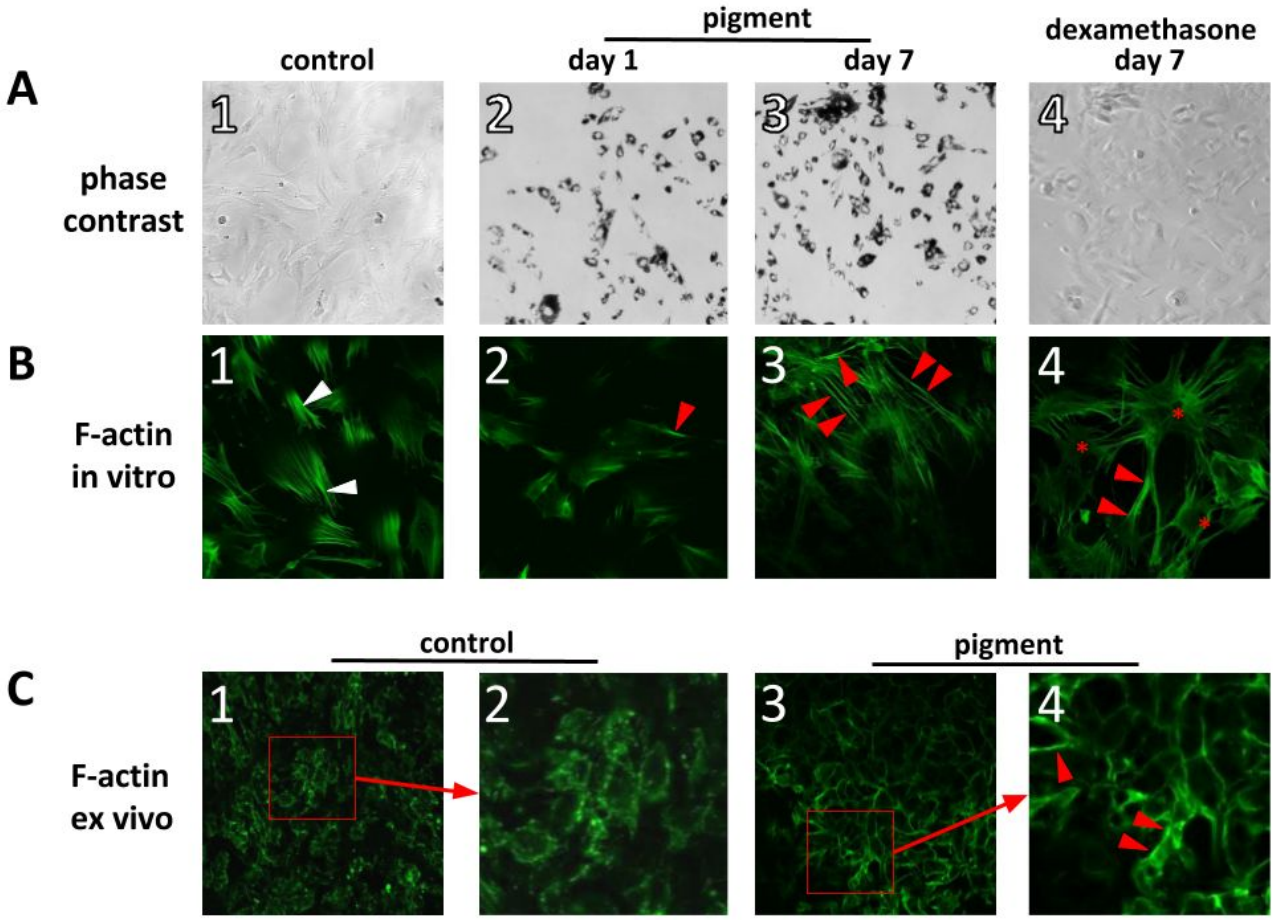

Figure 4. TM cytoskeletal changes induced by pigment. Primary TM cells exhibited typical spindle-like shapes (Figure 4A1) and did not show significantly morphological changes when exposed to pigment granules on day 1 (Figure 4A2) and day 7 (Figure 4A3). In contrast, dexamethasone used in positive control eyes induced a cell contraction by day 7 (Figure 4A4). F-actin, representative of cytoskeletal changes had fine, feather-like microfilaments cytoplasm of negative control TM cells (white arrows arrowheads, Figure 4B1). Pigment induced polymerization of actin filaments on day 1 (red arrowheads, Figure 4B2) and became long, thick, stress fibers on day 7 (red arrowheads, Figure 4B3). Dexamethasone induced similarly thick actin bundles on day 7 (red arrowheads, Figure 4B4), but with nest-like actin filaments (red star, Figure 4B4) rather than the cross-linked actin networks reported in human TM cells. The F-actin cytoskeleton of flat-mounted normal TM tissue showed weak and segmental structures (Figure 4C1-4C2), in contrast to thick, continuous stress fibers in the pigment group (Figure 4C3-4C4).

In vitro phagocytosis was measured by flow cytometry. Normal primary TM cells readily phagocytozed carboxylate-modified green-yellow microspheres. In contrast, cells exposed to pigment had a 5.17 fold decreased uptake (Fig. 5A; controls: 48.7±2.17%, pigment dispersion eyes 9.4±4.2%, P<0.001). We also developed a semiquantitative method to measure the ex vivo TM phagocytosis. Carboxylate-modified microspheres were perfused into the anterior chambers to be phagocytosed by TM cells in situ. Fluorescent intensity could be observed with an epifluorescence equipped dissecting microscope. The raw TM fluorescent intensity in the control group was $3.4\times10^{7}\pm4.5\times10^{6}$, significantly higher than that of the pigment group $2.2\times10^{7}\pm2.1\times10^{6}$ **(Fig. 5B, *P*=0.020)**.

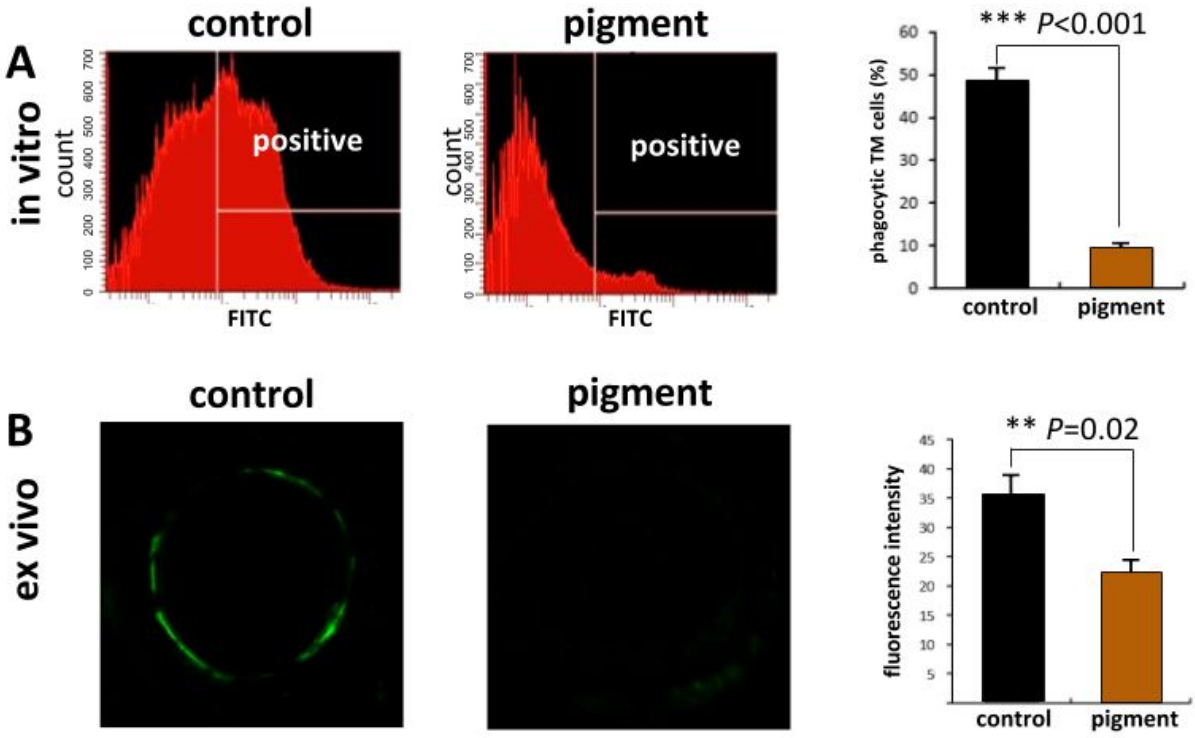

Figure 5. TM phagocytosis. In vitro TM phagocytosis was quantified with flow cytometry. Normal primary TM cells phagocytose fluorescent microspheres, but pigment dispersion have a 5.17-fold reduce uptake 48.73±2.17% versus 43±4.2%, P<0.001 (A). Ex vivo TM phagocytosis was quantified in a similar fashion but by measuring fluorescence of inverted anterior segments instead. Compared to controls, fluorescence was much lower ($3.4x10^7$±$4.5x10^6$ versus $2.2x10^7$±$2.1x10^6$, P= 0.020; **= P<0.01, ***= 0.001).

We also quantified the cell-matrix[29] and cell-cell adhesion[30]. Confluent TM monolayers that received pigment or vehicle treatment were subjected to trypsinization to measure the cell-matrix adhesion. The numbers of TM cells per visual field showed no significant difference between the two groups before trypsinization (230.00±5.51 in the pigment group versus 244.33±6.39 in controls, *P*=0.810). More TM cells in the pigment group started to contract, show shrinkage of the cell body, and detach after trypsinization. The remaining TM cells in the pigment group were significantly less than that of the control at the 2 minute ((173.33±10.81) vs (205.00±1.53), *P*=0.038) and 5 min mark (112.33±11.30 vs 158.67±6.94, *P*=0.010) **(Fig. 6, left band)**. For the cell-cell adhesion assay, confluent TM monolayers received pigment or vehicle treatment, were then scraped, digested, and counted. The ratio of cell aggregates to total single cells in the pigment group was slightly higher than the control, but not statistically different (Fig. 6,48.95±0.06 versus 43.30±0.04, *P*=0.462).

Cell migration was assessed by the numbers of cells which migrated into six-well plate from glass slides that were fully pre-populated with a TM monolayer. An average of 54583±8718 TM cells migrated onto the six-well plate after 10 days of pigment treatment, in contrast to 33000±5500 cells in the control group, however no statistical difference was found (*P* =0.078).

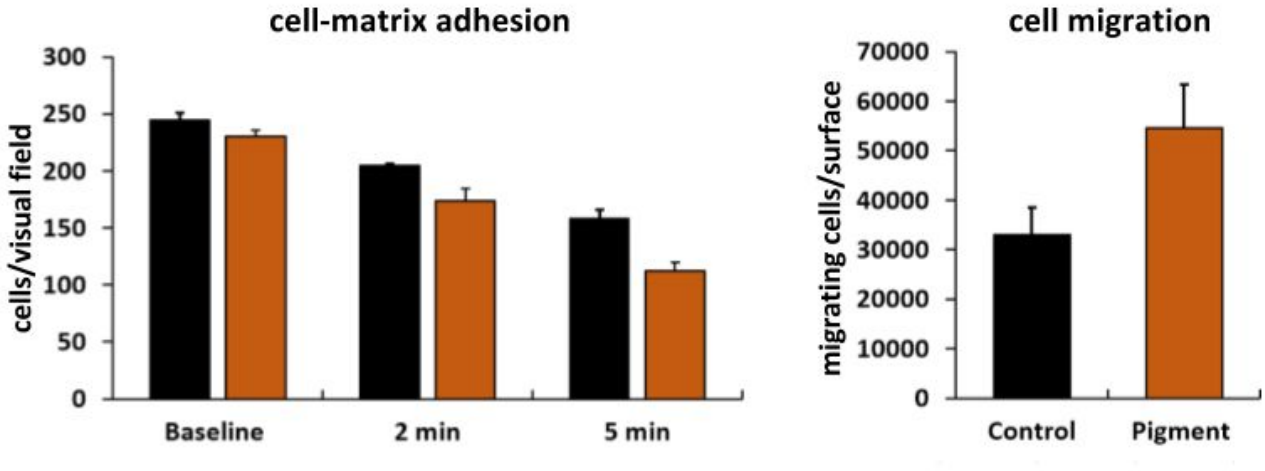

Figure 6. Cell adhesion and migration. Cell-matrix adhesion was quantified by trypsinization assay. Conflent TM monolayers were received either pigment or sham treatment, then were subjected to trypsinization. Number of TM cells per visual field showed no statistical difference at the baseline ((230.00±5.51) in the pigment group vs 244.33±6.39 in the control, P=0.810). TM cells treated by pigment were more sensitive to trypsinization and easier to detach than that of the control. The remaining TM cells were significantly less at the 2 minute ((173.33±10.81) vs (205.00±1.53), P = 0.038) and the 5 minute((112.33±11.30) vs (158.67±6.94), *P* = 0.010), compared to the control (Figure 6, left band). Cell migration was quantified by the numbers of TM cells migrating from the glass slide pre-populated by TM monolayer into six-well-plate. Compared to 33000±5500 in the control group, pigment treatment increased the average numbers of migrating TM cell to 54583.33±8718.20 after 10 days, but no statistical difference was found (*P*=0.231) (Figure 6, right band). * and ** represent P<0.05, and 0.01, respectively.

Pigment changes pathways of cellular movements, phagocytosis and aqueous outflow. Three TM samples from each group were submitted for Affymetrix Gene Microarray. A total of 24,123 *porcine* genes were analyzed, of which 691 were upregulated **(red dots in volcano plot Fig. 7A and red lines in heatmap Fig. 7B)** and 332 were downregulated **(green dots in volcano plot in Fig. 7A and green lines in heatmap Fig. 7B)** (Supplemental Table 1) more than 1.5 fold with statistical significance after pigment treatment (*P*<0.05).

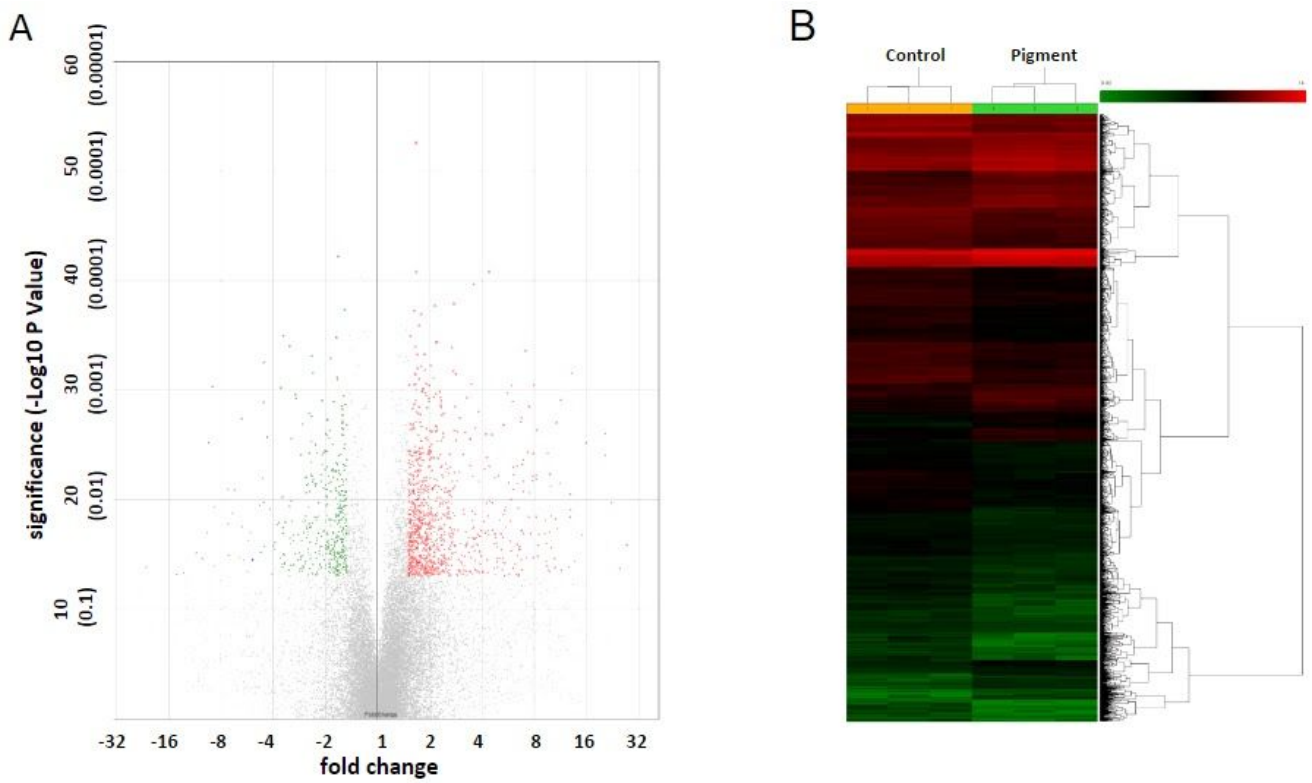

Figure 7: Differential gene expression by pigment treatment. Three TM samples from eyes that had a confirmed intraocular pressure elevation phenotype were compared to controls using the Affymetrix Gene 3' IVT Microarray. A total of 24,123 porcine genes were hybridized, of which 691 were upregulated (red dots in volcano plot and red lines in heatmap) and 332 were downregulated (green dots in volcano plot and green lines in heatmap) by more than 1.5 fold.

After excluding 239 porcine genes with unclear biological functions, 784 genes (Supplemental Table 2) were mapped in our pathway analysis to 16 distinct signal pathways that related to (1) cellular movement: cell adhesion, diapedesis and migration, (2) endocytosis and phagocytosis, (3) aqueous outflow facility, (4) oxidative stress and endoplasmic reticulum stress, and (5) TM extracellular matrix remodelling **(Fig. 8)**. RhoA signaling, the pivotal pathway that regulates the TM actin cytoskeleton was initialized by pigment treatment by a complex consisting of the insulin growth factor (IGF), the type 1 insulin-like growth factor receptor (IGF-IR) and the lysophosphatidic acid receptor (LPAR) in the cell membrane, differing from that of TGF β and its receptors induced-RhoA activation in POAG. Beside the direct inhibition of tight junction formation by RhoA activation, upregulation of rhophilin Rho GTPase binding protein (RHPN) also promoted the reorganization of TM actin cytoskeleton which negatively affected on tight junction protein 2/zonula occludens-associated nucleic acid binding protein complex, thus indirectly inhibit TM tight junction and clathrin, caveolar or Fc γ Receptor-mediated endocytosis and phagocytosis. Activation of RhoA signaling also enhanced myosin/MYBPH-mediated actin polarization, stress fiber formation and TM contractility which further affected to TM motility.

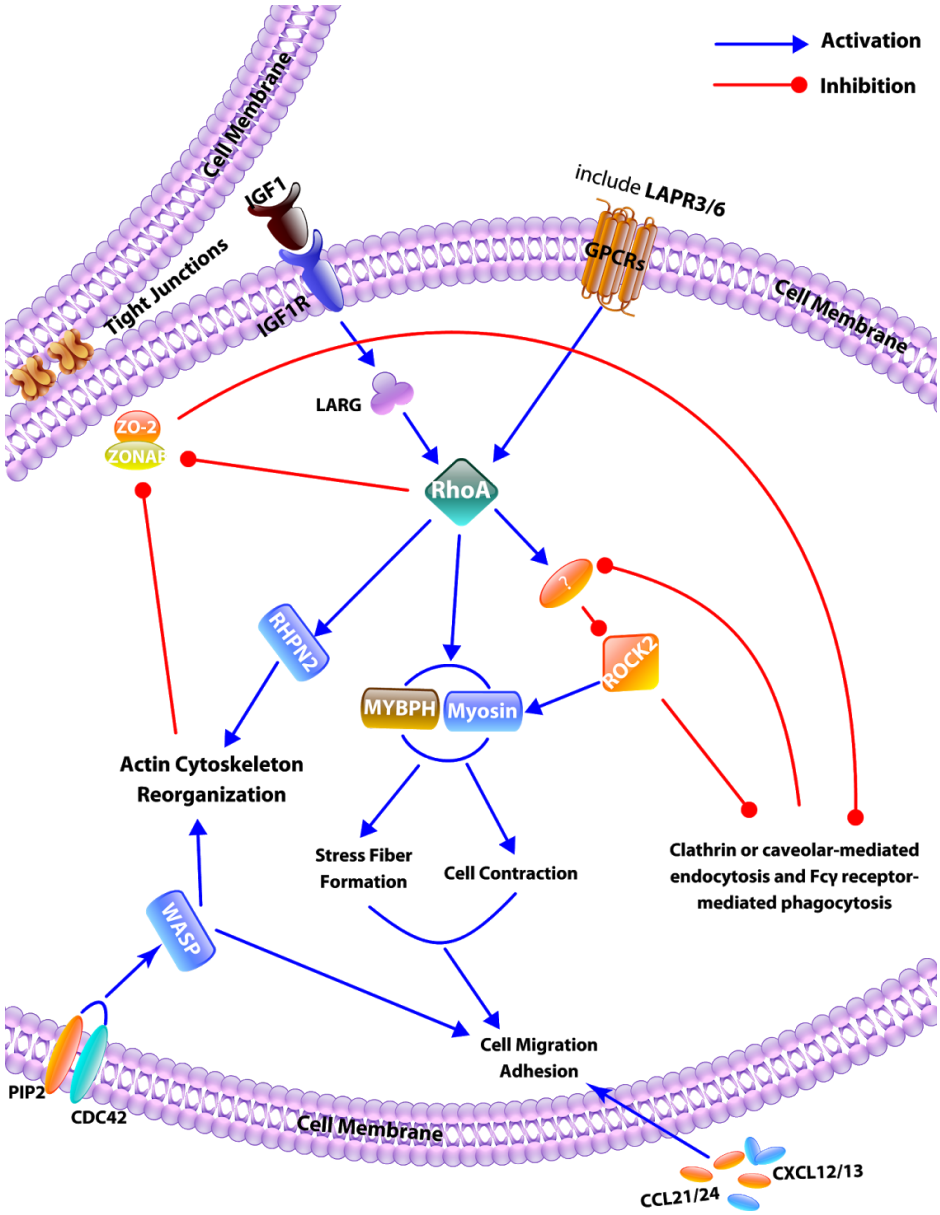

Figure 8. Intracellular signal transduction by pigment treatment. After exclusion of 239 genes with unknown functions, the rest of 784 differentially expressed genes were mapped by Ingenuity Pathway Analysis to 16 distinct signal pathways. RhoA signaling initialized by a complex consisting of the insulin growth factor (IGF), the type 1 insulin-like growth factor receptor (IGF-IR) and the lysophosphatidic acid receptor (LPAR) acts the central role. Activation of RhoA signaling inhibited tight junction protein 2/zonula occludens-associated nucleic acid binding protein complex (TJP2/ZONAB) mediated tight junction formation directly or through adjusting actin cytoskeleton reorganization by rhophilin Rho GTPase binding protein 2. Disruption of tight junction formation reduced the clathrin, caveolar or Fc γ receptor-mediated endocytosis and phagocytosis. Activation of RhoA signaling also promoted the stress fiber formation and TM contraction by myosin/MYBPH, thus further affected on TM motility. Additionally, TM motility by pigment treatment was regulated by a set of chemokine ligands (CCL21/CCL24 and CXCL12/CXCL13) on the cell membrane and their effectors in cytoplasm (Wiskott-Aldrich syndrome protein).

Additionally, the change of TM motility by pigment treatment can also be achieved through upregulation of a set of chemokine ligands (CCL21/CCL24 and CXCL12/CXCL13) in cell membrane and Wiskott-Aldrich syndrome protein in cytoplasm. Key genes, signal pathways are summarized in **Table 1** while their upstream regulators are listed in **Supplementary Table 2**.

Discussion

In this study, we developed an ex vivo model for pigmentary glaucoma (PG) to study TM function and signal pathway changes in order to identify new treatment targets for this common form of secondary glaucoma. Pig eyes developed the same hypertensive IOP phenotype and histological changes of human PG[20,21,31,32] when pigment was added to mimic pigment dispersion in patients. These are normally released from iris pigment epithelium by iridozonular contact and pupillary movement[33]. We developed a freeze-thaw method[34] to maintain epitopes and avoid chemicals and applied them to this structure. These pigment granules are similar to pigment in pigment dispersion, have a typical ovoid or circular shape with a mean size of 1.03±0.11 microns, are phagocytosed by TM cells and do not cause a physical obstruction of intertrabecular spaces[34]. As discussed in the following, these results suggest that the cause of high IOP in PG includes a reduced phagocytosis, stress fiber formation, and cell migration.

We isolated primary porcine TM cells to validated our ex vivo studies. These TM cells displayed the typical TM markers seen in human TM cells and readily phagocytozed particulate matter of similar size. Unchanged viability of the cells with a complete lack of cytotoxicity or induction of apoptosis when exposed to pigment dispersion convinced us to proceed with the ex vivo studies.

IOP started to diverge in eyes with continuous pigment dispersion at 48 hours and remained at a constant level thereafter. These eyes also displayed a larger range of IOPs when compared to controls, an observation that matches pigmentary glaucoma in human patients. The IOP elevation of 10 mmHg above baseline is within the range seen in a clinical setting, considerably less acute and high compared to angle closure models, thereby realistically reflecting the most common phenotype.

The ultrastructure and histological examination matched studies of human eyes. Most importantly, there was no physical obstruction to outflow but rather a relatively modest deposition of pigment within the TM and its cells. In anterior segments with pigment diffusion, TM cells were busy with phagocytosis and breakdown of ingested pigment granules. The TM cytoskeleton displayed stress fibers with polymerization of F-actin microfilaments. Different from the formation of cross-linked actin networks in other forms of glaucoma[35], for instance, steroid induced glaucoma[28] and POAG[36], the stress fibers in this model are typically long, thick, bundle-like microfilaments, suggesting distinct TM cytoskeletal alterations in PG. Human TM cells can form cross-linked actin networks (CLANs) within 7 days in steroid-induced ocular hypertension[28,35]. An acute disruption of F-actin was reported in latex microbead-induced phagocytic challenge of bovine TM cells[37]. TM cytoskeletal changes that directly affect the TM stiffness and outflow facility[38], have already previously been targeted in glaucoma medications: ROCK inhibitors[39] and NO donors[40] relax the TM. In contrast, dexamethasone[41], TGF-β 2[42] and senescence[43] result in an increased ECM stiffness and decreased outflow.

We developed a method for in situ visualization and quantitative analysis of TM phagocytosis. TM does not only regulate outflow but also prevents debris from entering the outflow system, phagocytoses particulate matter and presents it to the immune system[44]. Phagocytosis was reduced to 20% in pigment exposed TM cells. This appears to be similar to other secondary open angle glaucomas with an increased phagocytosis load, in particular ghost cell glaucoma[45], and steroid induced glaucoma[25]. The cell matrix adhesion decreased while their motility increased. Both are features of human PD and cause a decreased TM cellularity over time: migration of TM cells into SC has been reported in human PG[20,21] while the cell-matrix adhesion declined resulting in a reorganization of cytoskeletal structures[46]. This may explain why the pathology of TM in pigmentary glaucoma is so different from that of pigment dispersion syndrome[22]; a limited amount of pigment may cause no harm and will be degraded but if a threshold is exceeded, TM cells may migrate off the TM-ECM and potentially occlude the intertrabecular space or the downstream outflow tract. Gottanka et al[20] found

that SCs in human PG specimens were partly (25%-65%) obstructed by loosely arranged, distended cribriform TM cells.

The changes in intracellular signaling in our model highlight the pivotal role of RhoA and its activators IGF/IGF1R/LPAR in the molecular pathogenesis of PG. RhoA plays a central role in the actin cytoskeleton organization and cell motility[47] and has been observed in other glaucomas[48,49]. In our model, this differed from the TGF β induced-RhoA activation in POAG[48,49], suggesting a distinctly different mechanism. TM tight junctions are formed by the interaction between actin fibers and tight junction proteins. Junctional tightness and distribution influence aqueous outflow facility and adhesion - downregulation of CDLN2 may be related to increased cell migration[50]. Activation of RhoA caused a disruption of TM tight junctions by modulating actin stress fibers[51,52]. The downregulation of CLDN2 and ZO-2 is also seen after steroid exposure[52]. Normal tight junctions contribute to maintaining cell polarity, thereby allowing specialized surface functions such as receptor-mediated phagocytosis and endocytosis. Consistent with that we found that clathrin or the caveolar-mediated endocytosis pathways and the Fc γ receptor-mediated phagocytosis pathway were all significantly downregulated by the pigment exposure. Analysis of of signal pathway alteration in a PG model on such a fine scale may be used to pinpoint targets of future focus for research and ultimately therapeutic purposes.

In summary, we developed a PG model that manifested a hypertensive IOP phenotype as well as histological and ultrastructural characteristics similar to that of human PG. Pathway analysis revealed that activation of RhoA plays a pivotal role in the alteration of TM actin cytoskeleton, tight junction formation, phagocytosis, and cell motility which each may be provide a specific target for future PG treatment.

Methods

Generation of pigment

Ten fresh pig eyes obtained from a local abattoir (Thoma Meat Market, Saxonburg, PA) were sterilized and dissected within 2 hours of sacrifice. After removal of the posterior segment, lens, and ciliary body, the anterior segments were saved in plain DMEM for mounting. Irises were collected to produce pigment granules. The production of pigment granules employed two-step freeze-thaw cycles. Briefly, ten irises in 15 ml PBS were frozen at -80℃ for two hours, then thawed in the room temperature. After two cycles of freeze-thaw, tissue became fragile and pigment granules were shed from the irises through pipetting up and down 100 times with a 3ml Pasteur pipette. Pigment granules were filtered by a 70 μm cell strainer (cat#431751, Corning Incorporated, Durham, NC). After spinning at 3000 rpm for 15 min, supernatant was discarded and pigment granules were resuspended in 15 ml PBS and centrifuged again. Finally, the pellet was resuspended in 4 ml PBS and stored in 4℃ for up to 1 month to serve as a stock suspension.

The concentration of pigment granules was measured by a hemocytometer (cat#1490, Hausser Scientific, Horsham, PA). To calculate the size of pigment granules, the stock suspension was diluted 1000 times and visualized by a phase contrast microscope at 600 × magnification (Eclipse TE200-E, Nikon Instruments Inc., Melville, NY). At least 100 particles were measured for each batch of production.

TM primary culture

TM tissue from fresh pig eye was carefully dissected, sectioned into 0.5 mm^3 pieces, and maintained in a 37℃ humid CO_2 incubator with TM medium (OptiMEM (31985-070, Gibco, Life technologies, Grand Island, NY) supplemented with 5% FBS and 1% antibiotics (15240062, Thermo Fisher Scientific, Waltham, MA). After 100% confluence, the cells were passaged in a 1:3 ratio.

Primary TM cells were identified by immunostaining with TM specific antibodies. Briefly, the cells were fixed by 4% PFA for 1 hour, washed with PBS three times, and incubated with primary antibodies at 4℃ overnight: goat polyclonal matrix gla protein (MGP) antibody (1:100 dilution in PBS, sc-32820, Santa Cruz, Dallas, Texas), rabbit polyclonal anti alpha smooth muscle actin (α SMA) (1:100, ab5694, Abcam, Cambridge, MA) and aquaporin 1 (AQP1) antibodies (1:100, Sc-20810, Santa Cruz, Dallas, Texas). After three rinses of PBS, donkey-anti-goat Alexa Fluor® 647 (1: 1000, ab150131, Abcam, Cambridge, MA) and goat anti-rabbit IgG Superclonal™ secondary antibodies were added for 45 minutes in room temperature. Cell nuclei were counterstained by DAPI (D1306, Thermo Fisher Scientific, Waltham, MA). Pictures were taken by an upright laser scanning confocal microscope at 400 × magnification (BX61, Olympus, Tokyo, Japan).

Cell viability assay

Primary TM cells were plated into a six-well-plate at 1×10^5 cells per well and maintained with TM medium containing pigment granules at 1.67×10^7 particles/ml. TM medium without pigment served as a control. Medium was changed every 3 days for up to 10 days. Cells were stained with calcein AM (0.3 µM, C1430, Thermo Fisher, Waltham, MA) and PI (1 µg/ml, P1304MP, Thermo Fisher, Waltham, MA) for 30 minutes, followed by trypsinization and resuspension into 500 µl PBS for flow cytometry. Viable TM cells have intracellular esterase activity which can convert non-fluorescent calcein AM to green fluorescent calcein, but not allow red fluorescent PI to pass through the intact cell membrane and bind to the cell nucleus[23]. Thus, the calcein-labeled TM cells were counted as the viable cells while PI stained cells were dead or apoptotic cells.

Ex vivo pigmentary glaucoma model

Perfusion model: Fresh pig anterior segments were mounted and perfused with DMEM supplemented with 1% FBS and 1% antibiotics as described previously[12,34]. Baseline IOPs were obtained after 72 hours and pigment granules diluted with perfusion medium to a concentration of 1.67×10^7 particles/ml were perfused for 180 hours. Normal medium without pigment granules served as a control. IOPs were recorded at two minute intervals.

In vitro model: Primary TM cells treated with pigment containing media were utilized as an in vitro PG model and the control group was sham treated. Briefly, 3×10^5 primary TM cells were plated onto a 60 mm dish and maintained with OptiMEM supplemented with 5% FBS and 1% antibiotics for 24 hours and pigment granules were then added to the final concentration of 1.67×10^7 particles/ml. Medium was changed every three days. Normal TM medium without pigment served as a control.

Histology and transmission electron microscopy (TEM)

Anterior segments from perfusion culture were fixed with 4% paraformaldehyde for 24 hours, paraffin embedded, cut to 5 μm sections, and stained with hematoxylin and eosin for histology[12]. The ultrastructures of ex vivo TM tissue and in vitro cell monolayers were evaluated by transmission electron microscopy (TEM). Preparation of TEM samples followed a previous protocol with minor modification[53]. Briefly, the samples were pre-fixed with 2.5% glutaraldehyde in 0.05 M cacodylate buffer for 24 hours, washed with PBS three times and then postfixed with 1% osmium tetroxide solution overnight. After 3 rinses of PBS, samples were dehydrated through an ethanol series (30%, 50%, 70%, 90% and 100% ethanol, 45 minutes each), followed by embedding in Epon (Energy Beam Sciences, East Granby, CT). Epon was exchanged completely every hour for three hours and blocks were cured for 2 days at 60°C. 300 nm sections were obtained by Reichert-Jung Ultra-cut 701701 Ultra Microtome and stained with 0.5% Toluidine Blue O Solution (S25613, Thermo Fisher Scientific, Waltham, MA) to choose areas of interest. Ultrathin sections (65 nm) were obtained and placed on grids. After staining with uranyl acetate and lead citrate, pictures were taken under an 80 kV Jeol transmission electron microscope (Peabody, MA) at various magnifications.

Phagocytic activity

In vitro TM phagocytosis was quantified by percentages of TM cells that had engulfed fluorescent microspheres using flow cytometry. Briefly, carboxylate-modified yellow-green fluorescent microspheres (final concentration: 5×10^8 microspheres/ml, diameter: 0.5 micron, cat# F8813, Thermo Fisher, Waltham, MA) were incubated with the TM cells treated by pigment granules or sham treated for 1 hour. Cells were washed with PBS three times, trypsinized, and resuspended into 500 ul PBS for FACS analysis.

TM phagocytosis in situ was quantified by measuring TM fluorescent intensity after perfusion with carboxylate-modified yellow-green fluorescent microspheres for 24 hours. Briefly, 0.5 μm carboxylate-modified yellow-green fluorescent microspheres at 5×10^8 /ml were loaded to the perfusion system for 24 hours. Anterior chambers were washed three times with PBS. TM cells that had engulfed microspheres showed bright green fluorescence under a dissecting fluorescence microscope (SZX16, Olympus, Tokyo, Japan). Images were acquired at a 680 x 510 pixel resolution and a 1/17 second exposure. The raw TM fluorescent intensity was measured by ImageJ as previously described (Version 1.50i, NIH)[17,54].

TM cytoskeleton

F-actin and alpha SMA were used for assessing the cytoskeletal changes of TM in vitro and ex vivo. Ex vivo and in vitro TM samples were fixed by 4% PFA for 1 hour and washed with PBS three times. For F-actin staining, the samples were incubated with Alexa Fluor® 488 Phalloidin (1:40 dilution, A12379, Thermo Fisher, Waltham, MA) for 30 minutes and counterstained with DAPI. For alpha SMA staining, samples were incubated with rabbit polyclonal anti-alpha SMA antibody at 4℃ overnight, washed three times with PBS, and labeled by goat anti-rabbit IgG Superclonal™ secondary antibodies and DAPI respectively. Images were acquired under an upright laser scanning confocal microscope at 600× magnification (BX61, Olympus, Tokyo, Japan).

TM motility

Cell-matrix adhesion: cell-matrix adhesion was evaluated using a previous protocol with a minor modification[29]. Confluent TM monolayers treated with pigment granules or sham treated were washed with PBS and dissociated with 0.25% trypsin. The changes in cell morphology and adhesion were monitored by a phase-contrast microscope at different trypsinization time intervals (0 min, 2 min, and 5 min). The ratio of "numbers of attached TM cell" to "total TM cells" represents the cell-matrix adhesive ability.

Cell migration: primary TM cells were plated onto 18 mm^2 cover glasses (2855-18, Corning Incorporated, Durham, NC 27712). After 100% confluency, these cover glasses were transferred to six-well plates and maintained in TM medium with or without pigment granules (1.67 x 10^7 particles/ml). Medium was replaced every three days. Cover glasses were removed after ten days. Cells which migrated into each well from the cover glass were trypsinized and counted by a hemocytometer.

Gene microarray, qPCR and pathway analysis

Anterior segments (n=3 each) from the pigment treated and normal control groups were dissected after the ideal IOP phenotypes were obtained. Cells from TM tissues were lysed by Trizol Reagent (15596026, Invitrogen, Thermo Fisher, Waltham, MA). The lysates were sent to Genomic Core Facility of University of Pittsburgh for quantification control. Amplification and hybridization were performed using Affymetrix Porcine 3'IVT Array (900624, Affymetrix, Santa Clara, CA) which contains 23,937 probe sets to interrogate 23,256 transcripts in pig representing 20,201 *Sus scrofa* genes. The Affymetrix CEL files were extracted, normalized, and statistically analyzed by ANOVA using Transcriptome Analysis Console (TAC) (Version 3.1, Affymetrix, Santa Clara, CA). The differential gene expression profiles were characterized by volcano plots and heatmaps. The default filter criteria were (1) Fold Change (linear) < -1.5 or Fold Change (linear) > 1.5, and (2) ANOVA p-value < 0.05. Genes that matched these criteria were selected for bioinformatic pathway analysis using Ingenuity Pathway Analysis (Qiagen, Hilden, Germany).

Key gene expression was confirmed by qPCR[55]. Briefly, RNA was extracted and reverse transcribed into cDNA by High-Capacity cDNA Reverse Transcription Kit (4368814, Thermo Fisher Scientific, Waltham, MA). Quantitative PCR was performed on the StepOnePlus™ Real-Time PCR System (4376600, Thermo Fisher Scientific, Waltham, MA) according to the manufacturer's instructions. 2ul of cDNA (10ng/ul), 10ul of SYBR® Green PCR Master Mix, 4ul of primers (1000 nM) and 4ul of water were loaded into 96-well PCR plates. The initial denaturation lasted 10 min at 95°C, and cDNA was amplified for 40 cycles through 15 sec. denaturation at 95°C and 1 min. annealing and extension at 65°C. Primer sequences are listed in Table 1.

Statistics

Data was presented as mean±standard error. Differential gene expression was statistically analyzed by TAC (Version 3.1, Affymetrix, Santa Clara, CA). Other quantitative data was processed by One-way

ANOVA by PASW 18.0 (SPSS Inc., Chicago, IL, USA). Statistical difference was considered significant if $p<0.05$.

Acknowledgement

This study is supported by NEI K08-EY022737 (Nils A Loewen) and The Initiative to Cure Glaucoma of the Eye and Ear Foundation of Pittsburgh (Nils A Loewen).

Conflicts of Interest

The authors declare no conflict of interest.

References

1. De Moraes, C. G. & Susanna, R., Jr. in *Pearls of Glaucoma Management* (eds. Giaconi, J. A., Law, S. K., Nouri-Mahdavi, K., Coleman, A. L. & Caprioli, J.) 419–430 (Springer Berlin Heidelberg, 2016).
2. Niyadurupola, N. & Broadway, D. C. Pigment dispersion syndrome and pigmentary glaucoma - a major review. *Clin. Experiment. Ophthalmol.* **36,** 868–882 (2008).
3. Sugar, H. S. & Barbour, F. A. Pigmentary glaucoma; a rare clinical entity. *Am. J. Ophthalmol.* **32,** 90–92 (1949).
4. Ritch, R., Steinberger, D. & Liebmann, J. M. Prevalence of pigment dispersion syndrome in a population undergoing glaucoma screening. *Am. J. Ophthalmol.* **115,** 707–710 (1993).
5. Mardin, C. Y., Küchle, M., Nguyen, N. X., Martus, P. & Naumann, G. O. Quantification of aqueous melanin granules, intraocular pressure and glaucomatous damage in primary pigment dispersion syndrome. *Ophthalmology* **107,** 435–440 (2000).
6. John, S. W. *et al.* Essential iris atrophy, pigment dispersion, and glaucoma in DBA/2J mice. *Invest. Ophthalmol. Vis. Sci.* **39,** 951–962 (1998).
7. Marneros, A. G. & Olsen, B. R. Age-dependent iris abnormalities in collagen XVIII/endostatin deficient mice with similarities to human pigment dispersion syndrome. *Invest. Ophthalmol. Vis. Sci.* **44,** 2367–2372 (2003).
8. Chen, L., Zhao, Y. & Zhang, H. Comparative Anatomy of the Trabecular Meshwork, the Optic Nerve Head and the Inner Retina in Rodent and Primate Models Used for Glaucoma Research. *Vision Res.* **1,** 4 (2016).
9. Tripathi, R. C. Ultrastructure of the exit pathway of the aqueous in lower mammals:(A preliminary report on the 'angular aqueous plexus'). *Exp. Eye Res.* **12,** 311–314 (1971).
10. Sanchez, I., Martin, R., Ussa, F. & Fernandez-Bueno, I. The parameters of the porcine eyeball. *Graefes Arch. Clin. Exp. Ophthalmol.* **249,** 475–482 (2011).
11. Loewen, R. T. *et al.* Regionally Discrete Aqueous Humor Outflow Quantification Using Fluorescein Canalograms. *PLoS One* **11,** e0151754 (2016).
12. Loewen, R. T. *et al.* A Porcine Anterior Segment Perfusion and Transduction Model With Direct Visualization of the Trabecular Meshwork. *Invest. Ophthalmol. Vis. Sci.* **57,** 1338–1344 (2016).
13. McMenamin, P. G. & Steptoe, R. J. Normal anatomy of the aqueous humour outflow system in the

domestic pig eye. *J. Anat.* **178,** 65–77 (1991).

14. Dang, Y., Loewen, R., Parikh, H. A., Roy, P. & Loewen, N. A. Gene transfer to the outflow tract. *Exp. Eye Res.* 044396 (2016).
15. Loewen, R. T. *et al.* Quantification of Focal Outflow Enhancement Using Differential Canalograms. *Invest. Ophthalmol. Vis. Sci.* **57,** 2831–2838 (2016).
16. Parikh, H. A. *et al.* Differential Canalograms Detect Outflow Changes from Trabecular Micro-Bypass Stents and Ab Interno Trabeculectomy. *Sci. Rep.* **6,** 34705 (2016).
17. Dang, Y. *et al. Rapid learning curve assessment in an ex vivo training system for microincisional glaucoma surgery*. (PeerJ Preprints, 2017). doi:10.7287/peerj.preprints.2745v1
18. Wang, C. *et al.* Angle stability and outflow in excisional ab interno trabeculectomy with active versus passive chamber management. *PeerJ* (2017). doi:10.7287/peerj.preprints.2762v2
19. Fallano, K., Bussel, I., Kagemann, L., Lathrop, K. L. & Loewen, N. Training strategies and outcomes of *ab interno* trabeculectomy with the trabectome. *F1000Res.* **6,** (2017).
20. Gottanka, J., Johnson, D. H., Grehn, F. & Lütjen-Drecoll, E. Histologic findings in pigment dispersion syndrome and pigmentary glaucoma. *J. Glaucoma* **15,** 142–151 (2006).
21. Rohen, J. W. & van der Zypen, E. The phagocytic activity of the trabecularmeshwork endothelium. An electron-microscopic study of the vervet (Cercopithecus aethiops). *Albrecht Von Graefes Arch. Klin. Exp. Ophthalmol.* **175,** 143–160 (1968).
22. Campbell, D. G. & Schertzer, R. M. Pathophysiology of pigment dispersion syndrome and pigmentary glaucoma. *Curr. Opin. Ophthalmol.* **6,** 96–101 (1995).
23. Gonzalez, J. M., Jr, Hamm-Alvarez, S. & Tan, J. C. H. Analyzing live cellularity in the human trabecular meshwork. *Invest. Ophthalmol. Vis. Sci.* **54,** 1039–1047 (2013).
24. Tian, B., Geiger, B., Epstein, D. L. & Kaufman, P. L. Cytoskeletal involvement in the regulation of aqueous humor outflow. *Invest. Ophthalmol. Vis. Sci.* **41,** 619–623 (2000).
25. Zhang, X., Ognibene, C. M., Clark, A. F. & Yorio, T. Dexamethasone inhibition of trabecular meshwork cell phagocytosis and its modulation by glucocorticoid receptor beta. *Exp. Eye Res.* **84,** 275–284 (2007).
26. Matsumoto, Y. & Johnson, D. H. Trabecular meshwork phagocytosis in glaucomatous eyes. *Ophthalmologica* **211,** 147–152 (1997).

27. Saccà, S. C. *et al.* The Outflow Pathway: A Tissue With Morphological and Functional Unity. *J. Cell. Physiol.* **231,** 1876–1893 (2016).

28. Yuan, Y. *et al.* Dexamethasone induces cross-linked actin networks in trabecular meshwork cells through noncanonical wnt signaling. *Invest. Ophthalmol. Vis. Sci.* **54,** 6502–6509 (2013).

29. Zhou, L., Fukuchi, T., Kawa, J. E., Higginbotham, E. J. & Yue, B. Y. Loss of cell-matrix cohesiveness after phagocytosis by trabecular meshwork cells. *Invest. Ophthalmol. Vis. Sci.* **36,** 787–795 (1995).

30. Wecker, T., Han, H., Börner, J., Grehn, F. & Schlunck, G. Effects of TGF-β2 on cadherins and β-catenin in human trabecular meshwork cells. *Invest. Ophthalmol. Vis. Sci.* **54,** 6456–6462 (2013).

31. Alvarado, J. A. & Murphy, C. G. Outflow obstruction in pigmentary and primary open angle glaucoma. *Arch. Ophthalmol.* **110,** 1769–1778 (1992).

32. Campbell, D. G. & Schertzer, R. M. Pathophysiology of pigment dispersion syndrome and pigmentary glaucoma: Editorial review. *Curr. Opin. Ophthalmol.* **6,** 96–101 (1995).

33. Kupfer, C., Kuwabara, T. & Kaiser-Kupfer, M. The histopathology of pigmentary dispersion syndrome with glaucoma. *Am. J. Ophthalmol.* **80,** 857–862 (1975).

34. Dang, Y. *et al. Freeze-thaw decellularization of the trabecular meshwork in an ex vivo eye perfusion model*. (PeerJ Preprints, 2017). doi:10.7287/peerj.preprints.2736v1

35. O'Reilly, S. *et al.* Inducers of cross-linked actin networks in trabecular meshwork cells. *Invest. Ophthalmol. Vis. Sci.* **52,** 7316–7324 (2011).

36. Hoare, M.-J. *et al.* Cross-linked actin networks (CLANs) in the trabecular meshwork of the normal and glaucomatous human eye in situ. *Invest. Ophthalmol. Vis. Sci.* **50,** 1255–1263 (2009).

37. Zhou, L., Li, Y. & Beatrice Y J. Alteration of cytoskeletal structure, integrin distribution, and migratory activity by phagocytic challenge in cells from an ocular tissue—The trabecular meshwork. *In Vitro Cell.Dev.Biol.-Animal* **35,** 144–149 (1999).

38. Wang, K., Read, A. T., Sulchek, T. & Ethier, C. R. Trabecular meshwork stiffness in glaucoma. *Exp. Eye Res.* (2016). doi:10.1016/j.exer.2016.07.011

39. Daneshvar, R. & Amini, N. Rho-Associated Kinase Inhibitors: Potential Future Treatments for Glaucoma. *J. Ophthalmic Vis. Res.* **9,** 395–398 (2014).

40. Dismuke, W. M., Liang, J., Overby, D. R. & Stamer, W. D. Concentration-related effects of nitric oxide and

endothelin-1 on human trabecular meshwork cell contractility. *Exp. Eye Res.* **120,** 28–35 (2014).

41. Raghunathan, V. K. *et al.* Dexamethasone Stiffens Trabecular Meshwork, Trabecular Meshwork Cells, and Matrix. *Invest. Ophthalmol. Vis. Sci.* **56,** 4447–4459 (2015).
42. Welge-Lüssen, U., May, C. A. & Lütjen-Drecoll, E. Induction of tissue transglutaminase in the trabecular meshwork by TGF-beta1 and TGF-beta2. *Invest. Ophthalmol. Vis. Sci.* **41,** 2229–2238 (2000).
43. Morgan, J. T., Raghunathan, V. K., Chang, Y.-R., Murphy, C. J. & Russell, P. Wnt inhibition induces persistent increases in intrinsic stiffness of human trabecular meshwork cells. *Exp. Eye Res.* **132,** 174–178 (2015).
44. Morgan, J. T. *et al.* Human trabecular meshwork cells exhibit several characteristics of, but are distinct from, adipose-derived mesenchymal stem cells. *J. Ocul. Pharmacol. Ther.* **30,** 254–266 (2014).
45. Quigley, H. A. & Addicks, E. M. Chronic experimental glaucoma in primates. I. Production of elevated intraocular pressure by anterior chamber injection of autologous ghost red blood cells. *Invest. Ophthalmol. Vis. Sci.* **19,** 126–136 (1980).
46. Zhou, L., Li, Y. & Yue, B. Y. Alteration of cytoskeletal structure, integrin distribution, and migratory activity by phagocytic challenge in cells from an ocular tissue--the trabecular meshwork. *In Vitro Cell. Dev. Biol. Anim.* **35,** 144–149 (1999).
47. Sit, S.-T. & Manser, E. Rho GTPases and their role in organizing the actin cytoskeleton. *J. Cell Sci.* **124,** 679–683 (2011).
48. Fuchshofer, R. & Tamm, E. R. The role of TGF-β in the pathogenesis of primary open-angle glaucoma. *Cell Tissue Res.* **347,** 279–290 (2012).
49. Danias, J. *et al.* Gene expression changes in steroid-induced IOP elevation in bovine trabecular meshwork. *Invest. Ophthalmol. Vis. Sci.* **52,** 8636–8645 (2011).
50. Raviola, G. & Raviola, E. Paracellular route of aqueous outflow in the trabecular meshwork and canal of Schlemm. A freeze-fracture study of the endothelial junctions in the sclerocorneal angel of the macaque monkey eye. *Invest. Ophthalmol. Vis. Sci.* **21,** 52–72 (1981).
51. Bruewer, M., Hopkins, A. M., Hobert, M. E., Nusrat, A. & Madara, J. L. RhoA, Rac1, and Cdc42 exert distinct effects on epithelial barrier via selective structural and biochemical modulation of junctional proteins and F-actin. *Am. J. Physiol. Cell Physiol.* **287,** C327–35 (2004).

52. Zhuo, Y. H. *et al.* Dexamethasone disrupts intercellular junction formation and cytoskeleton organization in human trabecular meshwork cells. *Mol. Vis.* **16,** 61–71 (2010).

53. 667., 206. ELECTRON MICROSCOPY PROCEDURES MANUAL.

54. Schneider, C. A., Rasband, W. S. & Eliceiri, K. W. NIH Image to ImageJ: 25 years of image analysis. *Nat. Methods* **9,** 671–675 (2012).

55. Dang, Y. *et al.* Papaverine inhibits lipopolysaccharide-induced microglial activation by suppressing NF- κ B signaling pathway. *Drug Des. Devel. Ther.* **10,** 851–859 (2016).

54. Hu, D.-N. *et al.* Vascular endothelial growth factor is increased in aqueous humor of glaucomatous eyes. *J. Glaucoma* **11,** 406–410 (2002).